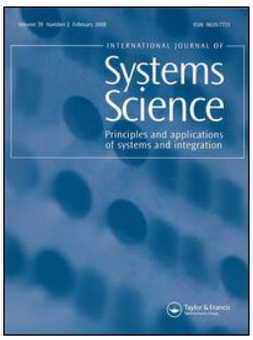

International Journal of Systems Science

ISSN: (Print) (Online) Journal homepage: https://www.tandfonline.com/loi/tsys20

Decentralised navigation systems for bearing-based position and velocity estimation in tiered formations

David Santos, Pedro Batista, Paulo Oliveira & Carlos Silvestre

To cite this article: David Santos, Pedro Batista, Paulo Oliveira & Carlos Silvestre (2021): Decentralised navigation systems for bearing-based position and velocity estimation in tiered formations, International Journal of Systems Science, DOI: 10.1080/00207721.2021.1961916

To link to this article: https://doi.org/10.1080/00207721.2021.1961916

Published online: 27 Aug 2021.

INTERNATIONAL JOURNAL OF SYSTEMS SCIENCE
https://doi.org/10.1080/00207721.2021.1961916

Taylor & Francis
Taylor & Francis Group

Decentralised navigation systems for bearing-based position and velocity estimation in tiered formations

David Santos[a], Pedro Batista[a,b], Paulo Oliveira[c*] and Carlos Silvestre[a,d,§]

[a]Institute for Systems and Robotics, Laboratory for Robotics and Engineering Systems, Lisboa, Portugal; [b]Instituto Superior Técnico, Universidade de Lisboa, Lisboa, Portugal; [c]LAETA-Associated Laboratory for Energy, Transports and Aeronautics, IDMEC-Institute of Mechanical Engineering, and Instituto Superior Técnico, Universidade de Lisboa, Lisboa, Portugal; [d]Faculty of Science and Technology, Department of Electrical and Computer Engineering, University of Macau, Taipa, Macau

ABSTRACT

This paper presents a novel decentralised navigation system based on bearing measurements for tiered vehicle formations. In the proposed framework, some vehicles have access to measurements of their own position, whereas others have access to bearing measurements to one or more neighbouring vehicles. Depth measurement may also be available. Local observers for the position and fluid velocity are designed based on the derivation of an equivalent observable linear time-varying system, thus yielding globally exponentially stable error dynamics. The local observers rely on local measurements, as well as limited communications between the vehicles. The stability of the system as a whole is analysed by studying the robustness of the local observers to exponentially decaying perturbations. Thorough Monte Carlo simulations are presented and discussed to compare the performance of the proposed solution with the extended Kalman filter, the unscented Kalman filter, and the Bayesian Cramér-Rao bound.

ARTICLE HISTORY
Received 12 May 2021
Accepted 25 July 2021

KEYWORDS
Bearings; navigation; decentralised estimation; Kalman filters; sensor fusion

1. Introduction

The use of formations is advantageous in many applications, see, for example, Healey (2001), Kopfstedt et al. (2008), and Pack et al. (2009), where vehicle formations are considered in surveillance and localisation. While centralised control and navigation systems are the most widely used due to their conceptual simplicity, decentralised solutions have many advantages. The most obvious of them is that the formation does not depend on a central node, which can compromise the whole application. Another disadvantage of centralised solutions is the need to communicate with each element of the formation. However, in underwater applications, communications are limited. Decentralised solutions may help to coping with this issue. In Vaccarani and Longhi (2009), Stilwell and Bishop (2000), Joordens and Jamshidi (2010), and Fonti et al. (2011), examples of decentralised solutions for underwater applications are proposed.

Due to electromagnetic waves attenuation, GPS systems are not available in underwater applications. As such, it is necessary to develop alternative navigation systems, such as the ones proposed in Techy et al. (2011) and Whitcomb et al. (1999). Most of the solutions available in the literature are based on the range measurements. However, it is possible to develop navigation systems based on bearing measurements. An ultra-short baseline acoustic positioning system, a sensor that provides bearing measurements, is developed and discussed in detail in Reis et al. (2016). A lot of work has been done with regard to navigation using bearing measurement, such as a study on the observability issues of target motion analysis based on the angle measurements, which was developed in Hammel and Aidala (1985). Particle filters based on bearing measurements are proposed in Zhang and Ji (2012) and Brehard and Cadre (2007), while in Zhao et al. (2014) a square cubature Kalman filter is presented.

CONTACT Pedro Batista pbatista@isr.tecnico.ulisboa.pt

*Present addresses: Institute for Systems and Robotics, Laboratory for Robotics and Engineering Systems, Lisboa, Portugal; Instituto Superior Técnico, Universidade de Lisboa, Lisboa, Portugal.

§On leave from the Instituto Superior Técnico, Universidade de Lisboa, 1049 001 Lisboa, Portugal.

In this paper, a novel decentralised filter for vehicle formations operating underwater is proposed. The formations are assumed to be tiered and acyclic, with the vehicles of the top tier having access to their own position due to, for example, the availability of a long-baseline system or GPS, for the case of surface vehicles. In the rest of the tiers, vehicles measure bearings and have communication with vehicles in the upper tier. Local state observers, capable of estimating the vehicle position and the surrounding fluid velocity, are designed. These local observers have access to bearing measurements and positions estimates communicated from the vehicles in the tier above. They also have access to several local measurements, such as attitude angles, velocity relative to the surrounding fluid and, in some cases, depth. Three different cases of local observers are considered: (i) when one bearing and depth are available; (ii) when one bearing is available but depth is not; and (iii) when two or more bearings, but no depth, are available. The proposed framework is of high applicability, e.g. when the vehicles are distributed in tiers in the water column and/or the horizontal plane, with limited communications and line-of-sight restrictions. In these scenarios, it is possible for vehicles that are in adjacent tiers to communicate, but not vehicles farther apart.

In Viegas et al. (2016), continuous-time decentralised range-based navigation systems are proposed for tiered acyclic formations. The local observers are based on a previous solution developed by the authors, see Batista et al. (2011), whereby the state is redefined such that equivalent linear time-varying systems are obtained, thus yielding GES error dynamics. To ensure that the decentralised system as whole exhibits globally exponentially stable (GES) error dynamics, the robustness of the local observers to exponentially decaying perturbations on the position estimates received through communication is analysed. This paper proposes a similar solution but based on bearing measurements instead of range measurements. Bearing measurements also lead to a system with nonlinear outputs. For such systems, the traditional solution is an extended Kalman filter (EKF). However, that does not offer any guarantee of stability. To obtain local observers with guarantees of GES error dynamics, an artificial output based on the bearing measurement can be used instead of the bearing itself, as in Batista et al. (2013b), where a continuous-time navigation system for single vehicles based on single bearing measurements is proposed. Since the bearing measurements and the communications are not available at a frequency high enough to consider a continuous-time system, the navigation system designed herein considers discrete-time kinematics. In Batista et al. (2013a), a similar solution to the one proposed in Batista et al. (2013b) is developed, but in a discrete-time context instead. In Batista et al. (2015), the previous work is extended to the case where multiple bearings are available. The present paper extends the previous results from single vehicles to tiered formations. This is, to the best of the authors' knowledge, the first time that cooperative decentralised navigation systems based on bearing measurements for tiered formations are proposed, with guarantees of global exponential stability.

Monte Carlo simulations are performed to compare the performance of the proposed solution with the EKF and the unscented Kalman filter (UKF). Also, the Bayesian Cramér-Rao Bound (BCRB), which gives the best achievable performance for an unbiased observer, is computed. The average error and root-mean-square error (RMSE) are presented to assess the existence of bias in the observers and the performance both in terms of convergence speed and steady-state variance. Also, an example where the proposed solution is the only converging is presented, which demonstrates the advantage of theoretical guarantees of stability over EKF- and UKF-based solutions, see, e.g. Hu et al. (2015), at no additional computational cost.

Previous work by the authors can be found in the 6-pages conference paper (Santos & Batista, 2020). The present work encompasses a comprehensive derivation of the solution. In addition to the proofs, which were omitted in the conference version, this paper also approaches the case where only one bearing measurement is available. Furthermore, it compares the performance of the proposed solution with the ones of the EKF, the UKF, as well as the BCRB, by resorting to Monte Carlo simulations. Besides this extensive comparison, the paper also introduces an example where only the proposed solution converges.

1.1. Notation

Throughout the paper, the symbol $\mathbf{0}$ denotes a matrix of 0s of proper dimensions and $\mathbf{I}_n$ denotes the $n \times n$ identity matrix. A block diagonal matrix is represented by $\mathrm{diag}(\mathbf{A}_1, \ldots, \mathbf{A}_n)$. The special orthogonal group is denoted by $SO(3) := \{\mathbf{X} \in \mathbb{R}^{3\times 3} : \mathbf{X}^{\mathrm{T}}\mathbf{X} =$

$\mathbf{I} \wedge \det(\mathbf{X}) = 1\}$ and the set of unit vectors is defined as $S(2) := \{\mathbf{x} \in \mathbb{R}^3 : \|\mathbf{x}\| = 1\}$. For $\mathbf{x} \in \mathbb{R}^3$, $\mathbf{x}^x$, $\mathbf{x}^y$ and $\mathbf{x}^z$ denote the first, second, and third component of $\mathbf{x}$, respectively. The transpose operator is defined as $(\cdot)^{\mathrm{T}}$.

2. Problem statement

Consider a formation of N vehicles, indexed from 1 to N. All the vehicles are evolving in a fluid whose velocity is assumed to have a time-invariant spatial distribution. Moreover, it is assumed that the velocity of the vehicles is small enough such that the velocity of the fluid can be considered constant for each vehicle. Since the vehicles may be operating in different regions of the space, it is assumed that the velocity of the fluid may differ from vehicle to vehicle. As so, $\mathbf{v}_{fi}(t) \in \mathbb{R}^3$ denotes the fluid velocity around vehicle i, expressed in a local inertial frame, $\{I\}$. The position of the vehicle i, expressed in $\{I\}$, is denoted by $\mathbf{p}_i(t) \in \mathbb{R}^3$.

Each vehicle is moving with a velocity relative to the fluid, measured by a relative velocity sensor, such as a Doppler velocity log (DVL), and denoted by $\mathbf{v}_i(t) \in \mathbb{R}^3$, expressed in the body frame, $\{B_i\}$. Each vehicle is also equipped with an attitude and heading reference system (AHRS) which provides a rotation matrix, $\mathbf{R}_i(t) \in SO(3)$, from $\{B_i\}$ to $\{I\}$.

The kinematics of vehicle i are given by

$$\begin{cases} \dot{\mathbf{p}}_i(t) = \mathbf{v}_{fi}(t) + \mathbf{R}_i(t)\mathbf{v}_i(t), \\ \dot{\mathbf{v}}_{fi}(t) = \mathbf{0}. \end{cases}$$

The formation is assumed to be organised in a tiered topology and each vehicle has access to either:

- An absolute position measurement, provided by, for example, GPS or a long baseline acoustic positioning system, if they are in the first tier; or
- Bearing measurements and position estimates of one or more vehicles in the tier above and, in some cases, depth measurements.

The focus of this paper is on the second case, since the position is available in the first one. In the second case, the outputs are available at discrete-time and are given by

$$\begin{cases} \mathbf{d}_{ij}(k) = \mathbf{R}_i^{\mathrm{T}}(t_k)\dfrac{\mathbf{p}_j(t_k) - \mathbf{p}_i(t_k)}{\|\mathbf{p}_j(t_k) - \mathbf{p}_i(t_k)\|}, \quad j \in D_i, \\ h_i(k) = \mathbf{p}_i^z(t_k), \quad \text{if depth available,} \end{cases}$$

where D_i is the set of vehicles to which vehicle i has bearing measurements and, to each discrete-time k, corresponds a continuous-time t_k.

From now on, and unless specified otherwise, it is considered

$$\mathbf{d}_{ij}(k) = \frac{\mathbf{p}_j(t_k) - \mathbf{p}_i(t_k)}{\|\mathbf{p}_j(t_k) - \mathbf{p}_i(t_k)\|}, \quad j \in D_i, \tag{1}$$

since this simplifies the computations. This is done without loss of generality since the matrix $\mathbf{R}_i(t_k)$ is available and invertible. For simulation purposes, the original bearing measurement is used.

Because the communication and the bearing measurements between vehicles are only available at low frequency, the system must be discretised, which leads to

$$\begin{cases} \mathbf{p}_i(t_{k+1}) = \mathbf{p}_i(t_k) + T\mathbf{v}_{fi}(t_k) + \mathbf{u}_i(k), \\ \mathbf{v}_{fi}(t_{k+1}) = \mathbf{v}_{fi}(t_k), \\ \mathbf{d}_{ij}(k) = \dfrac{\mathbf{p}_j(t_k) - \mathbf{p}_i(t_k)}{\|\mathbf{p}_j(t_k) - \mathbf{p}_i(t_k)\|}, \quad j \in D_i, \\ h_i(k) = \mathbf{p}_i^z(t_k), \quad \text{if depth available,} \end{cases} \tag{2}$$

where T is the sampling period and $\mathbf{u}_i(k)$ is given by

$$\mathbf{u}_i(k) = \int_{t_k}^{t_{k+1}} \mathbf{R}_i(t)\mathbf{v}_i(t)\,\mathrm{d}t. \tag{3}$$

The problem addressed in this paper is that of designing a decentralised observer, with globally exponentially stable error dynamics, for the position and local fluid velocity of each vehicle, $\mathbf{p}_i$ and $\mathbf{v}_{fi}$, respectively. The decentralised observer is composed of local observers, each one with access to the local measurements described before.

3. Local observer design

Depending on the available measurements, the design of a local observer for (2) differs. Three cases are discussed: (i) when one bearing and depth are available; (ii) when two or more bearings are available; and (iii) when one bearing without depth is available. The first and third cases are analysed in detail while, in the second, results obtained in Batista et al. (2015) are used. From now on, the study will be focused on the design of the local observer for vehicle i. To simplify the notation, the index i is omitted from this point

onward, resulting in the system

$$\begin{cases} \mathbf{p}(t_{k+1}) = \mathbf{p}(t_k) + T\mathbf{v}_f(t_k) + \mathbf{u}(k), \\ \mathbf{v}_f(t_{k+1}) = \mathbf{v}_f(t_k), \\ \mathbf{d}_j(k) = \dfrac{\mathbf{p}_j(t_k) - \mathbf{p}(t_k)}{\|\mathbf{p}_j(t_k) - \mathbf{p}(t_k)\|}, \quad j \in D, \\ h(k) = \mathbf{p}^z(t_k), \quad \text{if depth available.} \end{cases} \tag{4}$$

3.1. Artificial output

The dynamic system (4) is nonlinear due to the bearing outputs. To address this issue and obtain a linear time-varying (LTV) system, the bearing outputs are replaced by artificial ones. First, note that

$$\mathbf{d}_j(k)\mathbf{d}_j^{\mathrm{T}}(k)\mathbf{d}_j(k) = \mathbf{d}_j(k)$$

since $\mathbf{d}_j(k)$ is a unit vector, from which it is possible to write

$$(\mathbf{I} - \mathbf{d}_j(k)\mathbf{d}_j^{\mathrm{T}}(k))\mathbf{d}_j(k) = \mathbf{0}. \tag{5}$$

Substituting the last term $\mathbf{d}_j(k)$ of (5) using the third equation of (4) leads to

$$(\mathbf{I} - \mathbf{d}_j(k)\mathbf{d}_j^{\mathrm{T}}(k))(\mathbf{p}_j(t_k) - \mathbf{p}(t_k)) = \mathbf{0}.$$

From this, $\mathbf{z}_j(k) \in \mathbb{R}^3$ is defined as

$$\begin{aligned} \mathbf{z}_j(k) &:= (\mathbf{I} - \mathbf{d}_j(k)\mathbf{d}_j^{\mathrm{T}}(k))\mathbf{p}_j(t_k) \\ &= (\mathbf{I} - \mathbf{d}_j(k)\mathbf{d}_j^{\mathrm{T}}(k))\mathbf{p}(t_k). \end{aligned}$$

This quantity is known since $(\mathbf{I} - \mathbf{d}_j(k)\mathbf{d}_j^{\mathrm{T}}(k))\mathbf{p}_j(t_k)$ can be computed using known measurements. Also, because $\mathbf{d}_j(k)$ is a known measurement, $\mathbf{z}_j(k)$ is linear on the state $\mathbf{p}(k)$. Replacing $\mathbf{d}_j(k)$ by $\mathbf{z}_j(k)$ in (4) yields

$$\begin{cases} \mathbf{p}(t_{k+1}) = \mathbf{p}(t_k) + T\mathbf{v}_f(t_k) + \mathbf{u}(k), \\ \mathbf{v}_f(t_{k+1}) = \mathbf{v}_f(t_k), \\ \mathbf{z}_j(k) = (\mathbf{I} - \mathbf{d}_j(k)\mathbf{d}_j^{\mathrm{T}}(k))\mathbf{p}(t_k), \quad j \in D, \\ h(k) = \mathbf{p}^z(t_k), \quad \text{if depth available.} \end{cases} \tag{6}$$

This is an LTV system and can be written in the form

$$\begin{cases} \mathbf{x}(k+1) = \mathcal{A}_k\mathbf{x}(k) + \mathcal{B}_k\mathbf{u}(k), \\ \mathbf{y}(k) = \mathcal{C}_k\mathbf{x}(k), \end{cases}$$

where

$$\mathbf{x}(k) = [\mathbf{p}^{\mathrm{T}}(t_k)\ \mathbf{v}^{\mathrm{T}}(t_k)]^{\mathrm{T}} \in \mathbb{R}^6,$$

and $\mathbf{y}(k)$ is the output, corresponding to the stacked measurements $\mathbf{z}_j(k)$, $j \in D$, and the depth measurement, when available.

3.2. Observability

3.2.1. One bearing and depth

When studying the system with only one bearing available, the index j will be omitted in $\mathbf{d}_j(k)$. The state matrices when depth and only one bearing measurement are available and given by

$$\mathcal{A}_k = \begin{bmatrix} \mathbf{I}_3 & T\mathbf{I}_3 \\ \mathbf{0} & \mathbf{I}_3 \end{bmatrix} \in \mathbb{R}^{6\times 6}, \quad \mathcal{B}_k = \begin{bmatrix} \mathbf{I}_3 \\ \mathbf{0} \end{bmatrix} \in \mathbb{R}^{6\times 3},$$

$$\mathcal{C}_k = \begin{bmatrix} \mathbf{I}_3 - \mathbf{d}(k)\mathbf{d}^{\mathrm{T}}(k) & \mathbf{0} \\ \mathbf{e}_3^{\mathrm{T}} & \mathbf{0} \end{bmatrix} \in \mathbb{R}^{4\times 6},$$

with $\mathbf{e}_3 := [0\ 0\ 1]^{\mathrm{T}}$.

The following theorem addresses the observability of this system.

Theorem 3.1: *The system* (6) *with depth and only one bearing available is observable on the interval* $[k_a, k_a + 2]$ *if and only if* $\mathbf{d}^z(k_a) \neq 0 \text{and} \mathbf{d}^z(k_a + 1) \neq 0$.

Proof: The system is observable on $[k_a, k_a + 2]$ if and only if the observability matrix $\mathcal{O}(k_a, k_a + 2)$ has rank equal to the number of states. The proof follows by showing that is the case. The observability matrix is given by

$$\mathcal{O}(k_a, k_a + 2) = \begin{bmatrix} \mathcal{C}_{k_a} \\ \mathcal{C}_{k_a+1}\mathcal{A}_{k_a} \end{bmatrix} \in \mathbb{R}^{8\times 6}.$$

The rank condition on the observability matrix is equivalent to state that the only solution of

$$\mathcal{O}(k_a, k_a + 2)\mathbf{c} = \mathbf{0}$$

is $\mathbf{c} = \mathbf{0}$. Considering $\mathbf{c} = [\mathbf{c}_1^{\mathrm{T}}\ \mathbf{c}_2^{\mathrm{T}}]^{\mathrm{T}}$, with $\mathbf{c}_1, \mathbf{c}_2 \in \mathbb{R}^3$, this can be rewritten as

$$\begin{cases} (\mathbf{I} - \mathbf{d}(k_a)\mathbf{d}^{\mathrm{T}}(k_a))\mathbf{c}_1 = \mathbf{0}, \\ \mathbf{c}_1^z = 0, \\ (\mathbf{I} - \mathbf{d}(k_a + 1)\mathbf{d}^{\mathrm{T}}(k_a + 1))(\mathbf{c}_1 + T\mathbf{c}_2) = \mathbf{0}, \\ \mathbf{c}_1^z + T\mathbf{c}_2^z = 0. \end{cases} \tag{7}$$

The sufficiency of the conditions of the theorem is shown by direct proof. Suppose $\mathbf{d}^z(k_a) \neq 0$ and $\mathbf{d}^z(k_a + 1) \neq 0$. Next, it is shown that the only solution for (7) is $\mathbf{c} = \mathbf{0}$. The first equation of (7) allows to conclude that $\mathbf{c}_1 = \alpha\mathbf{d}(k_a)$, $\alpha \in \mathbb{R}$. Since $\mathbf{d}^z(k_a) \neq 0$ and $\mathbf{c}_1^z = 0$, it must be $\alpha = 0$ and thus $\mathbf{c}_1 = \mathbf{0}$. Then, the

last two equations of (7) become

$$\begin{cases} (\mathbf{I} - \mathbf{d}(k_a+1)\mathbf{d}^{\mathrm{T}}(k_a+1))\mathbf{c}_2 = \mathbf{0}, \\ \mathbf{c}_2^z = 0. \end{cases}$$

Following the same steps, it can be concluded that $\mathbf{c}_2 = \mathbf{0}$. This concludes the proof of sufficiency. The proof of necessity follows by contraposition. Suppose that the conditions of the theorem are not met. This may happen because $\mathbf{d}^z(k_a) = 0$ or $\mathbf{d}^z(k_a+1) = 0$. In the first case, take

$$\mathbf{c} = \begin{bmatrix} \mathbf{d}(k_a) \\ -\frac{1}{T}\mathbf{d}(k_a) \end{bmatrix}.$$

This nonzero $\mathbf{c}$ fulfils (7), which makes the system not observable. Suppose now that $\mathbf{d}^z(k_a+1) = 0$ and take

$$\mathbf{c} = \begin{bmatrix} \mathbf{0} \\ \mathbf{d}(k_a+1) \end{bmatrix}.$$

This nonzero $\mathbf{c}$ also fulfils (7), which implies that the system is not observable, thus concluding the proof of necessity. ■

Remark 3.1: The conditions of the theorem are easy to achieve, considering the tiered topology of the formations. If the tiers are related to the vertical spatial distribution, being any tier deeper than the upper tier, then these conditions are always met. If the conditions are not met during a finite interval of time, state observers may diverge. However, once the observability conditions are satisfied again, state observers will converge again. Notice also that the system may be observable for longer time intervals even if this particular observability condition is not met, making using, for instance, of the richness of the trajectory, as detailed in Section 3.2.3.

3.2.2. Multiple bearings

When more than one bearing is available but there is no depth measurement, the state matrices are given by

$$\mathcal{A}_k = \begin{bmatrix} \mathbf{I}_3 & T\mathbf{I}_3 \\ \mathbf{0} & \mathbf{I}_3 \end{bmatrix} \in \mathbb{R}^{6\times 6}, \quad \mathcal{B}_k = \begin{bmatrix} \mathbf{I}_3 \\ \mathbf{0} \end{bmatrix} \in \mathbb{R}^{6\times 3},$$
$$\mathcal{C}_k = \begin{bmatrix} \mathbf{I}_3 - \mathbf{d}_1(k)\mathbf{d}_1^{\mathrm{T}}(k) & \mathbf{0} \\ \vdots & \vdots \\ \mathbf{I}_3 - \mathbf{d}_L(k)\mathbf{d}_L^{\mathrm{T}}(k) & \mathbf{0} \end{bmatrix} \in \mathbb{R}^{3L\times 6},$$

where L is the number of vehicles in D. This system has been studied in Batista et al. (2015), from where the following theorem can be used.

Theorem 3.2: *The system* (6) *with more than one bearing and no depth measurement is observable on the interval* $[k_a, k_a+2]$ *if and only if there exist* $m, n, l, p \in \{1, \ldots, L\}$ *such that*

$$\mathbf{d}_m(k_a) \neq \alpha_1 \mathbf{d}_n(k_a)$$

and

$$\mathbf{d}_l(k_a+1) \neq \alpha_2 \mathbf{d}_p(k_a+1)$$

for all $\alpha_1, \alpha_2 \in \mathbb{R}$.

Remark 3.2: To fulfil the condition of the theorem, even if only two bearings are available, it is enough that the vehicle of the system and the two vehicles to which the bearings are measured are not aligned. Even though this might not be the case, both conditions are not hard to achieve. Notice also that the present theorem considers two consecutive time instants, which is the most strict case. Nevertheless, observability can be achieved over longer periods, with different directions over non-consecutive discrete time instants.

3.2.3. One bearing without depth

When only one bearing is available and there is no depth measurement, the state space matrices are given by

$$\mathcal{A}_k = \begin{bmatrix} \mathbf{I}_3 & T\mathbf{I}_3 \\ \mathbf{0} & \mathbf{I}_3 \end{bmatrix} \in \mathbb{R}^{6\times 6}, \quad \mathcal{B}_k = \begin{bmatrix} \mathbf{I}_3 \\ \mathbf{0} \end{bmatrix} \in \mathbb{R}^{6\times 3},$$
$$\mathcal{C}_k = \begin{bmatrix} \mathbf{I}_3 - \mathbf{d}(k)\mathbf{d}^{\mathrm{T}}(k) & \mathbf{0} \end{bmatrix} \in \mathbb{R}^{3\times 6}.$$

The following theorem addresses the observability of this system.

Theorem 3.3: *The system* (6) *with only one bearing available is observable on the interval* $[k_a, k_a+3]$ *if and only if* $\mathbf{d}(k_a)$, $\mathbf{d}(k_a+1)$, *and* $\mathbf{d}(k_a+2)$ *are linearly independent.*

Proof: The system is observable on $[k_a, k_a+3]$ if and only if the observability matrix $\mathcal{O}(k_a, k_a+3)$ has rank equal to the number of states. The proof follows by showing that is the case. The observability matrix is

given by

$$\mathcal{O}(k_a, k_a+3) = \begin{bmatrix} \mathcal{C}_{k_a} \\ \mathcal{C}_{k_a+1}\mathcal{A}_{k_a} \\ \mathcal{C}_{k_a+2}\mathcal{A}_{k_a+1}\mathcal{A}_{k_a} \end{bmatrix} \in \mathbb{R}^{9\times 3}.$$

The rank condition on the observability matrix is equivalent to state that the only solution of

$$\mathcal{O}(k_a, k_a+3)\mathbf{c} = \mathbf{0}$$

is $\mathbf{c} = \mathbf{0}$. Considering $\mathbf{c} = [\mathbf{c}_1^{\mathrm{T}}\ \mathbf{c}_2^{\mathrm{T}}]^{\mathrm{T}}$, with $\mathbf{c}_1, \mathbf{c}_2 \in \mathbb{R}^3$, this can be rewritten as

$$\begin{cases} (\mathbf{I} - \mathbf{d}(k_a)\mathbf{d}^{\mathrm{T}}(k_a))\mathbf{c}_1 = \mathbf{0}, \\ (\mathbf{I} - \mathbf{d}(k_a+1)\mathbf{d}^{\mathrm{T}}(k_a+1))(\mathbf{c}_1 + T\mathbf{c}_2) = \mathbf{0}, \\ (\mathbf{I} - \mathbf{d}(k_a+2)\mathbf{d}^{\mathrm{T}}(k_a+2))(\mathbf{c}_1 + 2T\mathbf{c}_2). \end{cases} \tag{8}$$

The sufficiency of the conditions of the theorem is shown by direct proof. Suppose $\mathbf{d}(k_a)$, $\mathbf{d}(k_a+1)$, and $\mathbf{d}(k_a+2)$ are linearly independent. Next, it is shown that the only solution of (8) is $\mathbf{c} = \mathbf{0}$. To that purpose, notice that (8) allows to conclude that

$$\begin{cases} \mathbf{c}_1 = \alpha_1\mathbf{d}(k_a), \\ \mathbf{c}_1 + T\mathbf{c}_2 = \alpha_2\mathbf{d}(k_a+1), \\ \mathbf{c}_1 + 2T\mathbf{c}_2 = \alpha_3\mathbf{d}(k_a+2), \end{cases} \tag{9}$$

for $\alpha_1, \alpha_2, \alpha_3 \in \mathbb{R}$. Adding the first equation of (9) to the third and subtracting the second equation twice leads to

$$0 = \alpha_1\mathbf{d}(k_a) - 2\alpha_2\mathbf{d}(k_a+1) + \alpha_3\mathbf{d}(k_a+2). \tag{10}$$

Since the three bearing vectors are linearly independent, the only solution of (10) is $\alpha_1 = \alpha_2 = \alpha_3 = 0$. From (9), it follows that the only solution of (8) is $\mathbf{c}_1 = \mathbf{c}_2 = \mathbf{0}$, concluding the proof of sufficiency. The proof of necessity follows by contraposition. Suppose that the conditions of the theorem are not met. In this case, it is possible to choose $\boldsymbol{\alpha} = [\alpha_1\ \alpha_2\ \alpha_3] \neq \mathbf{0}$ such that

$$\alpha_1\mathbf{d}(k_a) + \alpha_3\mathbf{d}(k_a+2) = 2\alpha_2\mathbf{d}(k_a+1). \tag{11}$$

With such choice, take

$$\mathbf{c} = \begin{bmatrix} \alpha_1\mathbf{d}(k_a) \\ \dfrac{\alpha_3}{T}\mathbf{d}(k_a+2) - \dfrac{\alpha_2}{T}\mathbf{d}(k_a+1) \end{bmatrix}.$$

Then $\mathbf{c}$ fulfils (9) and, therefore, fulfils (8). If $\mathbf{c} \neq \mathbf{0}$, then the system is not observable and the proof of necessity would be concluded. Next, it is shown that the chosen $\boldsymbol{\alpha}$ and $\mathbf{c}$ imply $\mathbf{c} \neq 0$. The only case where $\mathbf{c} = \mathbf{0}$ is when $\alpha_1 = 0$ and $\alpha_2\mathbf{d}(k_a+1) = \alpha_3\mathbf{d}(k_a+2)$. Then, Equation (11) becomes

$$\alpha_1\mathbf{d}(k_a) = \alpha_2\mathbf{d}(k_a+1).$$

Since $\alpha_1 = 0$, then $\alpha_2 = 0 = \alpha_3$. This contradicts the hypothesis $\boldsymbol{\alpha} \neq \mathbf{0}$. Therefore, $\mathbf{c} \neq \mathbf{0}$, which concludes the proof of the theorem. ■

Remark 3.3: Among the three cases considered in this paper, the conditions of this theorem are the most restrictive since they require a trajectory rich enough such that the bearing is always changing. The smallest possible interval was considered in the theorem for single bearings. Nevertheless, observability can be achieved for longer time intervals.

With the observability studied, the design of a local linear Kalman filter (LKF) is the obvious choice, since it is applied to a system that is linear in the state. This is due to the fact that $\mathbf{d}_j$ is known. The Kalman filter yields globally exponentially stable error dynamics if the system is shown to be uniformly completely observable (Jazwinski, 1970). The proof, while long and tedious, follows similar steps considering uniform bounds in time, resulting in a version of the observability conditions that are uniform in time, see e.g. Batista et al. (2013b). Hence, it is omitted in the paper.

4. Decentralised system

4.1. Filter stability

The conditions for stability of the local observers have already been established. However, in the design of these local observers, it is assumed that the vehicles have access to the position of the vehicles to which bearings are measured. When the observers are put together into a decentralised system, they will only have access to position estimates, which can be written as

$$\hat{\mathbf{p}}_j(t_k) = \mathbf{p}_j(t_k) + \mathbf{e}_j(k),$$

where $\hat{\mathbf{p}}_j(t_k)$ is an estimate of the position of vehicle j and $\mathbf{e}_j(k)$ is a term with GES dynamics, which represents the estimation error of $\mathbf{p}_j(t_k)$. This will change

the value of the artificial output, which will be given by

$$\mathbf{z}_j(k) = (\mathbf{I} - \mathbf{d}_j(k)\mathbf{d}_j^{\mathrm{T}}(k))\mathbf{p}(t_k) + \bar{\mathbf{e}}_j(k), \tag{12}$$

where $\bar{\mathbf{e}}_j(k)$ is defined as

$$\bar{\mathbf{e}}_j(k) = (\mathbf{I} - \mathbf{d}_j(k)\mathbf{d}_j^{\mathrm{T}}(k))\mathbf{e}_j(k).$$

Since $\mathbf{e}_j(k)$ decays exponentially and $\mathbf{I} - \mathbf{d}_j(k)\mathbf{d}_j^{\mathrm{T}}(k)$ is bounded, $\bar{\mathbf{e}}_j(k)$ will also decay exponentially.

As so, the effect of not having the true position of the other vehicles can be regarded as an exponentially decaying perturbation on the outputs of system (6). This will not impact on the dynamics of the Kalman filter covariance matrix

$$\begin{cases} \mathbf{P}_{k|k-1} = \mathcal{A}_k \mathbf{P}_{k-1|k-1}\mathcal{A}_k^{\mathrm{T}} + \mathbf{Q}, \\ \mathbf{K}_k = \mathbf{P}_{k|k-1}\mathcal{C}_k^{\mathrm{T}}(\mathbf{R} + \mathcal{C}_k\mathbf{P}_{k|k-1}\mathcal{C}_k^{\mathrm{T}})^{-1}, \\ \mathbf{P}_{k|k} = (\mathbf{I} - \mathbf{K}_k\mathcal{C}_k)\mathbf{P}_{k|k-1}(\mathbf{I} - \mathbf{K}_k\mathcal{C}_k)^{\mathrm{T}} + \mathbf{K}_k\mathbf{R}_k\mathbf{K}_k^{\mathrm{T}}, \end{cases}$$

where $\mathbf{P}$ is the estimation error covariance, $\mathbf{K}$ is the observer gain, and $\mathbf{Q}$ and $\mathbf{R}$ are the process and output noise covariance matrices, respectively. Since these equations are not affected by the perturbation, they will remain bounded. The estimates will be given by

$$\hat{\mathbf{x}}(k+1) = \mathcal{A}_k\hat{\mathbf{x}}(k) + \mathcal{B}_k\mathbf{u}(k) + \mathbf{K}_k(\mathbf{z}(k) - \mathcal{C}_k\hat{\mathbf{x}}(k)).$$

Considering (12), the exponentially decaying perturbation will be multiplied by a bounded matrix, $\mathbf{K}$, which will cause an exponentially decaying error on the estimate of the state $\hat{\mathbf{x}}$.

4.2. Chain propagation

All the local observers of the vehicles of the second tier receive true information of the position of the vehicles of the tier above since it is assumed that the first tier has access to its own position. Therefore, they will produce estimates of their own position with GES error dynamics. As shown before, all the vehicles receiving position estimates with GES error dynamics will also produce positions estimates with GES error dynamics of their own. As so, the observers of all the tiers will converge, since the errors that are propagated will always have GES error dynamics.

5. Simulation results

Monte Carlo simulations were performed to assess the performance of the proposed solution when the measurements are subject to noise. A decentralised EKF and a decentralised UKF for the original system (2) was used for comparison, since this system is nonlinear. The BCRB was also computed, which provides a theoretical performance bound. Finally, an example where the EKF and the UKF diverge due to bad initialisation but the proposed solution converges is presented as a way to demonstrate the advantage of establishing theoretical guarantees of convergence.

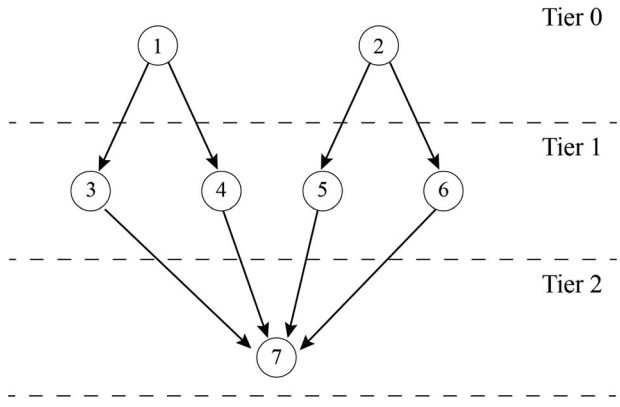

Figure 1. Formation graph.

5.1. Setup

To perform the simulations, the formation depicted in Figure 1 was used. The vehicles in tier 1 measure bearing to one of the vehicles in tier 0, as depicted in Figure 2. Vehicles 3, 4, and 5 measure depth but vehicle 6 does not. The vehicle in tier 2 measures bearing to all four vehicles of tier 1, as depicted in Figure 2, and has no access to depth measurements. The vehicles that measure bearings to other vehicles receive, through communications, the position estimates of those vehicles, as depicted in Figure 2. Each vehicle in tiers 1 and 2 implements, in the proposed solution. a LKF. Notice that, compared to a centralised solution, the amount of communications is significantly reduced, since no central node receives all the information and the vehicles in each tier only communicate with the vehicles in adjacent tiers.

All the vehicles perform the same type of trajectory but with different starting points. The trajectory was generated with way points, which are described in Table 1. The acceleration was limited to 0.01 m/s^2, which resulted in the curve presented in Figure 3. For vehicle 2, the trajectory followed the same curve of the other vehicles, to which it was added $[10\sin(0.1t)\ \ 50\cos(0.13)\ \ 0]^{\mathrm{T}}$. This is done to enrich

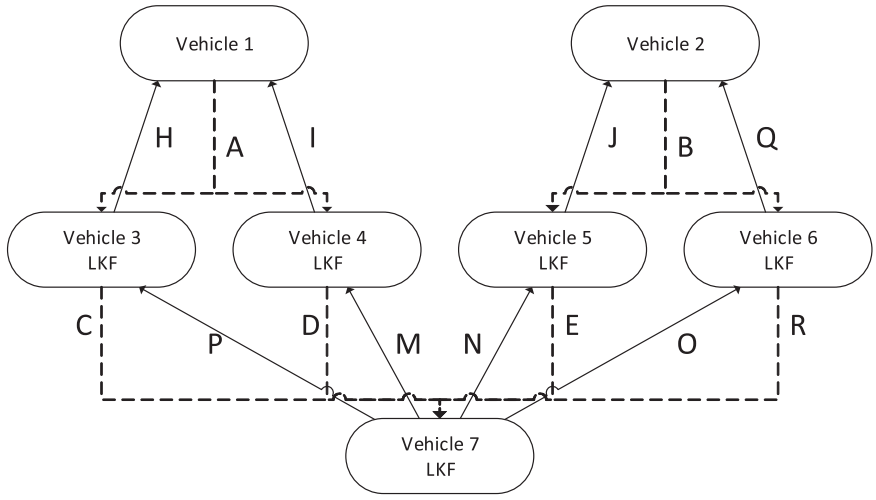

Figure 2. Communications (in dashed lines) and bearing measurements (in solid lines).

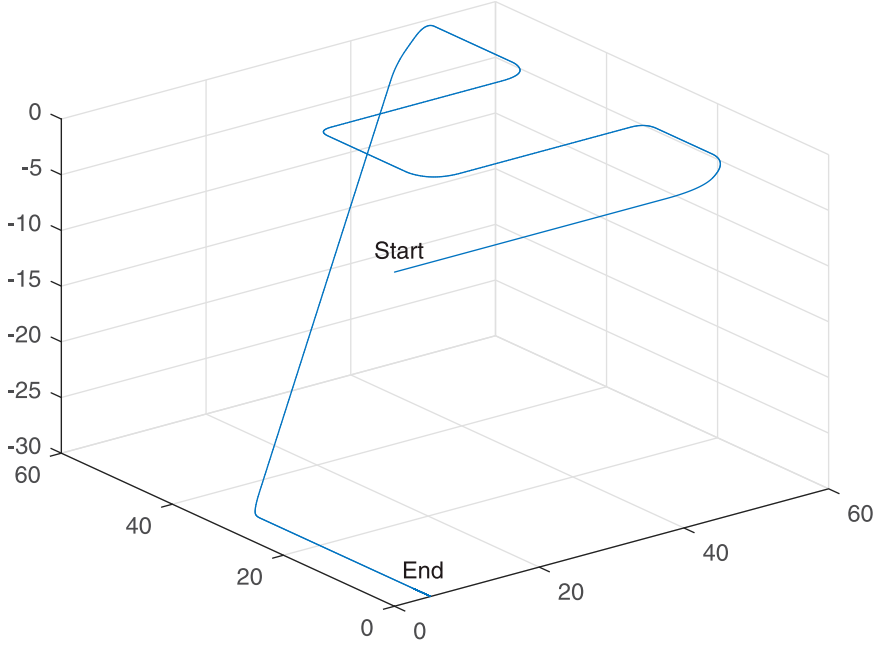

Figure 3. Trajectory for vehicle 1.

Table 1. Trajectory waypoints for vehicle 1.

Time (s)	Position (m)
0	[0 0 0]
100	[50 0 0]
200	[50 20 0]
300	[20 20 0]
400	[20 40 0]
500	[50 40 0]
600	[50 60 0]
800	[5 30 −30]
1000	[5 0 −30]

the bearing values of vehicle 6 relative to vehicle 2, so that the system becomes observable.

The fluid velocities were chosen with different values for each vehicle. The starting points and the fluid velocities are presented in Table 2. The fluid velocity for the first two vehicles was not specified since the observers for the upper tier were not simulated. This is done without loss of generality since the observers of tier 0 do not depend on the rest of the formation.

A sampling period of 1 s is assumed for both the bearing measurements and the communications between the vehicles, while all the other measurements are assumed to be available at 100 Hz. Azimuth and inclination are measured, from which the bearings are obtained as $\mathbf{d} = [\sin(\theta)\cos(\phi)\ \ \sin(\theta)\sin(\phi)\ \ \cos(\theta)]^{\mathrm{T}}$, where ϕ and θ are, respectively, the azimuth and inclination angles to another vehicle. Zero-mean white

Table 2. Initial positions and fluid velocities used in the simulations.

Vehicle	Initial position (m)	Fluid velocity (m/s)
1	[0 0 0]	–
2	[100 100 0]	–
3	[1 1 −50]	[0.19 0.13 0.30]
4	[0 10 −60]	[0.20 0.10 0.30]
5	[110 100 −40]	[0.18 0.11 0.28]
6	[90 90 −30]	[0.21 0.10 0.27]
7	[50 50 −100]	[0.21 0.12 0.27]

Gaussian noise with a standard deviation of 1 was added to both angles. For the vehicles in tier 0, the position is available but zero-mean white Gaussian noise was added with a standard deviation of 0.1 m in each component. Some correlation was added, resulting in the covariance matrix

$$0.01 \times \begin{bmatrix} 1 & 0.1 & 0.1 \\ 0.1 & 1 & 0.1 \\ 0.1 & 0.1 & 1 \end{bmatrix}.$$

Zero-mean white Gaussian noise with a standard deviation of 0.1 m was added to the depth measurements. For the Euler angles used to obtain the rotation matrix, uncorrelated zero-mean white Gaussian noise was added with a standard deviation of 0.01 for the pitch and roll angles and 0.03 for the yaw angle. Finally, the relative velocity to the fluid was corrupted by uncorrelated zero-mean white Gaussian noise with standard deviation of 0.01 m/s. The integral in (3) was computed using the trapezoidal rule.

5.2. Bayesian Cramér-Rao bound

Consider a system of the form of

$$\begin{cases} \mathbf{x}(k+1) = \mathbf{A}(k)\mathbf{x}(k) + \mathbf{B}(k)\mathbf{u}(k) + \mathbf{n}_x(k), \\ \mathbf{y}(k) = \mathbf{h}(\mathbf{x}(k)) + \mathbf{n}_y(k), \end{cases} \tag{13}$$

where $\mathbf{x}(k)$ is the state, $\mathbf{u}(k)$ is a deterministic input, and $\mathbf{y}(k)$ is the output, which depends on the state through a nonlinear function $\mathbf{h}(\mathbf{x}(k))$. Both $\mathbf{n}_x(k)$ and $\mathbf{n}_y(k)$ follow a zero-mean Gaussian distribution with covariance matrices $\mathbf{Q}_x(k)$ and $\mathbf{Q}_y(k)$, respectively. For a system in this form, the BCRB is provided in van Trees (2007), which is a lower bound on the estimation error achievable by any unbiased estimator.

The recursion used to compute the BCRB is the same as the one in the EKF, with the difference that the Jacobian of $\mathbf{h}$ is evaluated at the true state instead of the state estimate.

The original system (2) is not in the form of (13) since the noise is not added to the state and output of the system directly. However, the original system can be obtained from another system, where the outputs are the inclination and azimuth angles, instead of the bearing, as given by

$$\begin{cases} \mathbf{p}(t_{k+1}) = \mathbf{p}(t_k) + T\mathbf{v}_f(t_k) + \mathbf{u}(k), \\ \mathbf{v}_f(t_{k+1}) = \mathbf{v}_f(t_k), \\ \theta_j(k) = \arccos\left(\dfrac{\mathbf{p}_j^z(t_k) - \mathbf{p}^z(t_k)}{\|\mathbf{p}_j(t_k) - \mathbf{p}(t_k)\|}\right), \quad j \in D, \\ \phi_j(k) = \arctan\left(\dfrac{\mathbf{p}_j^y(t_k) - \mathbf{p}^y(t_k)}{\mathbf{p}_j^x(t_k) - \mathbf{p}^x(t_k)}\right), \quad j \in D, \\ h(k) = \mathbf{p}^z(t_k), \quad \text{if depth available.} \end{cases} \tag{14}$$

Not considering the noise present in the attitude angles nor in $\mathbf{p}_j$, (14) is in the form of (13), with the output noise being the one in the depth measure and the azimuth and inclination angles and the noise in the state being the one in the fluid velocity measure. As so, any unbiased observer for (2) should perform worse than the BCRB. However, due to nonlinearities, it is possible that the observers designed could result slightly biased.

5.3. Monte Carlo simulations

To check the performance of the proposed solution, Monte Carlo simulations were performed. A total of 1000 simulations were carried out. The developed solution consists of a Kalman Filter for (6) for each vehicle. The state covariance matrices were set to $\text{diag}(0.01^2\mathbf{I}, 0.001^2\mathbf{I})$, while the output covariance matrices were set to $\text{diag}(0.1^2, 10\mathbf{I})$ or $10\mathbf{I}$, depending on the availability of depth measurements. As for the decentralised EKF and for the decentralised UKF, which were implemented for comparison purposes, the state and output covariance matrices were set to, respectively, $\text{diag}(0.01^2\mathbf{I}, 0.001^2\mathbf{I})$ and $\text{diag}(0.1^2, 0.001\mathbf{I})$ or $0.001\mathbf{I}$, also depending on the availability of depth measurement. The generation of sigma-points used for the UKF followed the parametrisation proposed in Wan and Merwe (2000), with parameters $\alpha = 1$, $k = 0$ and $\beta = 2$.

For each of the 1000 simulations, different, randomly generated noise signals were considered, as

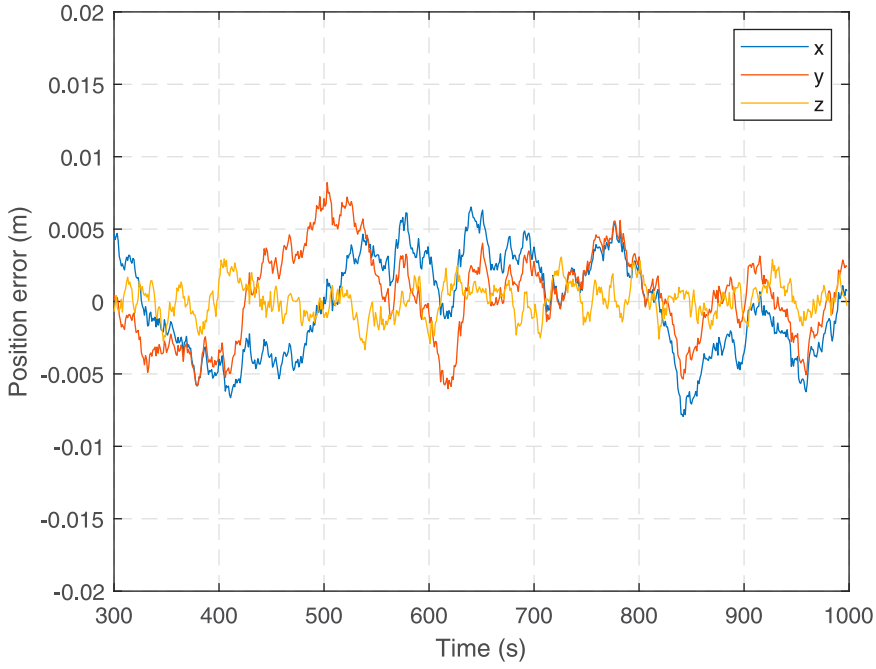

Figure 4. Vehicle 3: Average position error with the LKF.

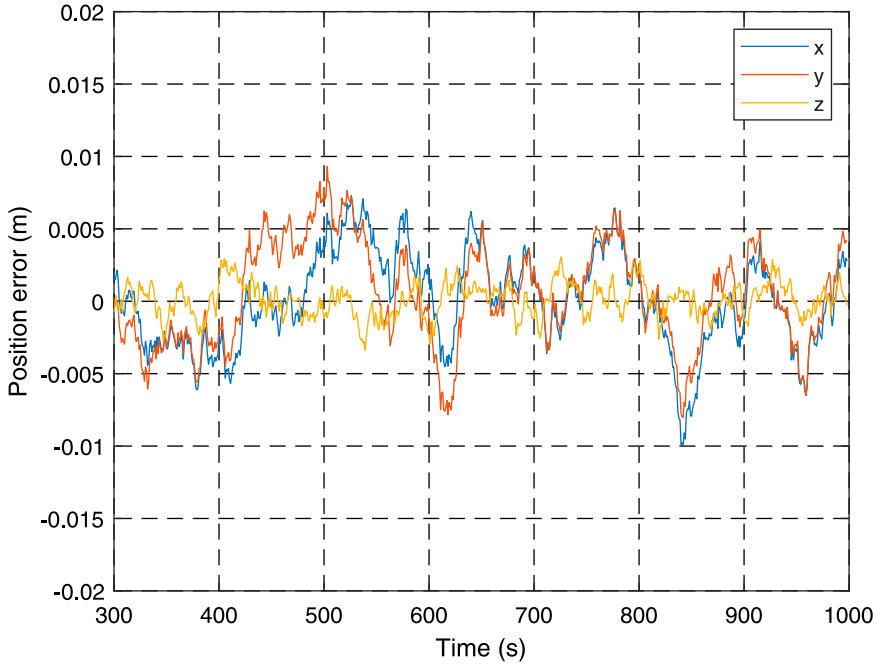

Figure 5. Vehicle 3: Average position error with the EKF.

detailed before. The initial state estimate was randomly generated from a Gaussian distribution centred about the true initial state and with covariance matrix $\mathrm{diag}(10^2\mathbf{I}, \mathbf{I})$. For all the solutions, the estimates converged for all the states of all vehicles.

To check the existence of bias, the mean of the estimation error for each time instant was computed. Only the results for vehicle 3 are displayed since the results for the remaining vehicles are analogous. In Figures 4–6, the mean of position estimation errors for the LKF, EKF, and UKF, respectively, are presented. It is possible to see that there is no significant bias and that the estimates fluctuate around zero. There is also little difference between the three filters.

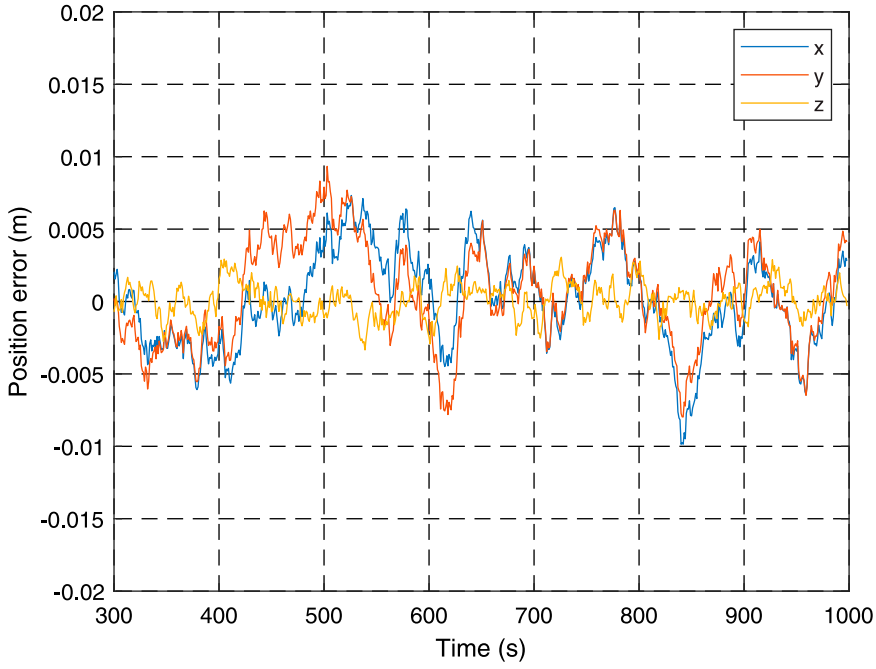

Figure 6. Vehicle 3: Average position error with the UKF.

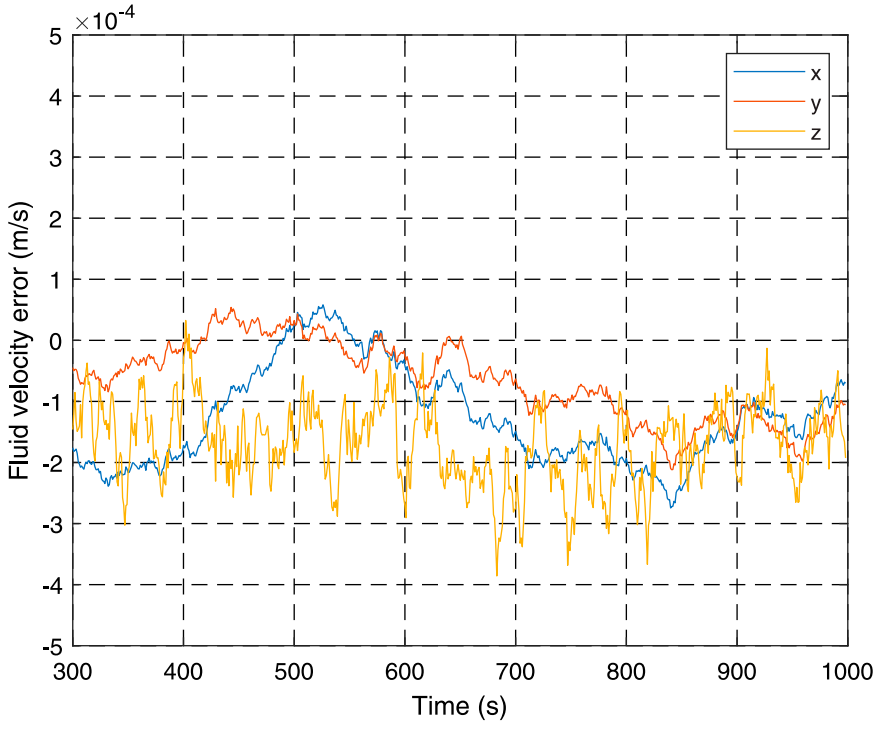

Figure 7. Vehicle 3: Average fluid error with the LKF.

In Figures 7–9, the mean of the fluid velocity estimation errors for the LKF, EKF, and UKF, respectively, are presented. There is a clear bias in the z component, which is caused by the nonlinearities of the simulated system. This bias is of similar value in all the solutions.

To analyse the variance of both solutions, the RMSE of the Monte Carlo simulations was computed. The results are presented for each component for vehicles 3, 6 and 7. The RMSE is a more meaningful performance metric and the results for each type of system

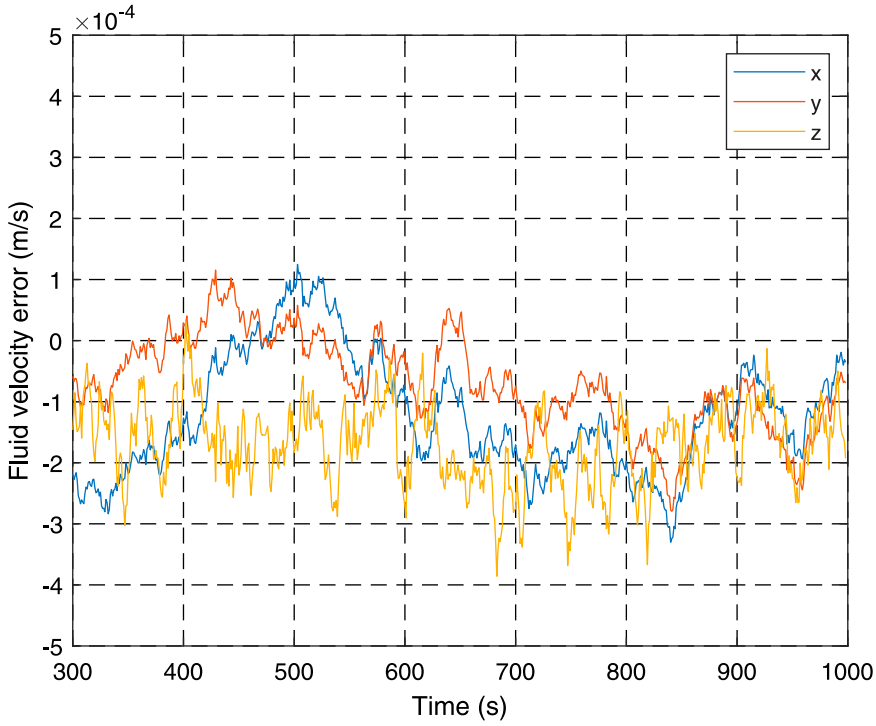

Figure 8. Vehicle 3: Average fluid error with the EKF.

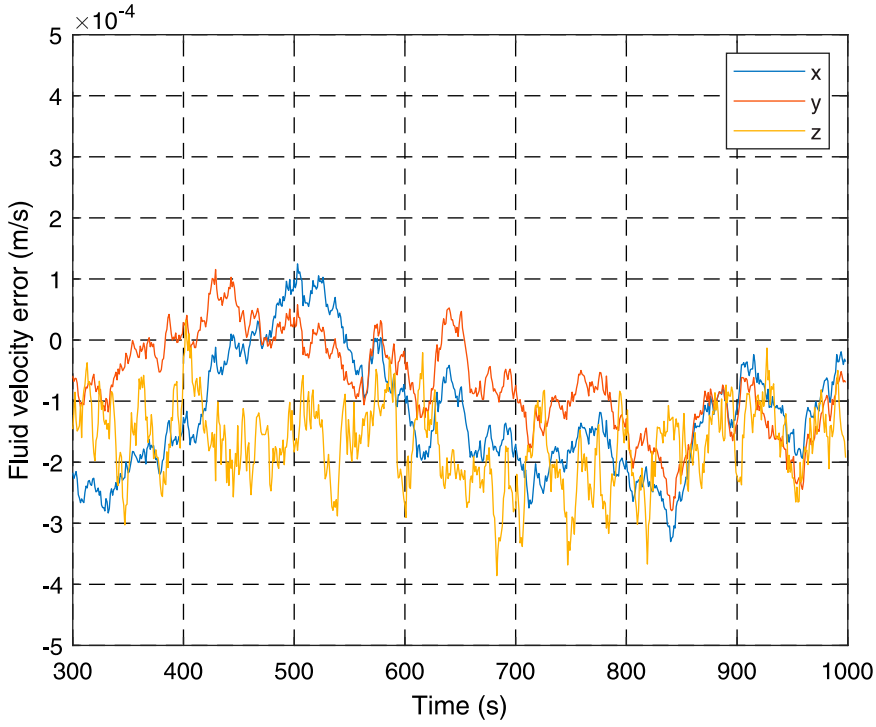

Figure 9. Vehicle 3: Average fluid error with the UKF.

are presented. In Figures 10–12, the RMSE of the position estimates for vehicle 3 can be seen for the x, y, and z components, respectively. The UKF is slightly faster to converge, followed by the LKF. The x and y components converge as fast as the BCRB until they reach steady-state, at which point the LKF reaches

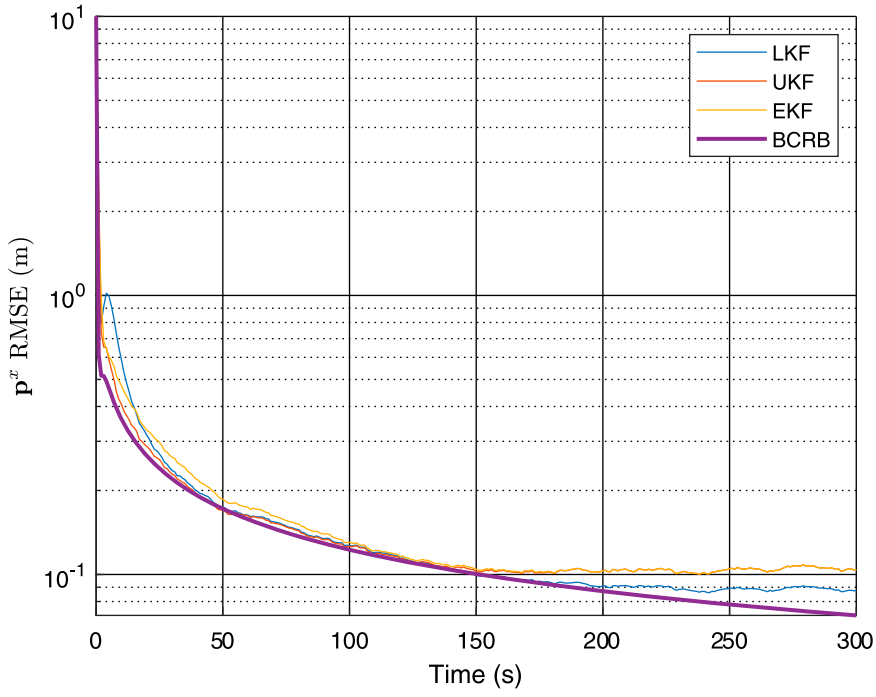

Figure 10. Vehicle 3: *x* component of position RMSE.

lower values. The *z* component presents the same behaviour for all the solutions, which was expected since this component is linearly available through the depth measurement.

In Figures 13–15, the RMSE of the fluid velocity estimates for vehicle 3 can be seen for the *x*, *y*, and *z* components, respectively. Conclusions identical to the position analysis can be drawn.

In Figures 16–18, the RMSE of the position estimates for vehicle 6 can be seen for the *x*, *y*, and *z* components, respectively. This time, it is clear that the LKF is slower to converge and none of the solutions converge as fast as the BCRB. However, it is interesting to see that all of them follow the same type of curve as the BCRB. The results for the fluid velocity of vehicle 6 are not presented since they do not bring any relevant information.

In Figures 19–21, the RMSE of the positions estimates for vehicle 7 can be seen for the *x*, *y*, and *z* components, respectively. The speed of convergence is similar for all the solutions but one interesting thing to note is that now the LKF, EKF, and UKF do not follow the same type of curve as the BCRB. This happens because the BCRB does not take into account errors introduced by the previous tier estimates, which are particularly noticeable during the initial transients.

To evaluate the steady-state error variance, the average of the RMSE from $t = 400$ s onwards was computed. The results are shown in Tables 3–7. For all the states, the average RMSE is higher for the EKF and UKF than for the proposed solution. At the same time, all are higher than the BCRB (square-rooted), as expected. Even though the proposed solution performs better in steady-state than the EKF, the differences are not significant.

Table 3. Vehicle 3: Steady-state error standard deviations.

	Position (m)			Fluid velocity (mm/s)		
	x	*y*	*z*	*x*	*y*	*z*
LKF	0.0871	0.0869	0.0332	0.9023	0.8924	1.7060
EKF	0.1030	0.1029	0.0332	1.4917	1.4839	1.7060
UKF	0.1030	0.1029	0.0332	1.4916	1.4839	1.7060
BCRB	0.0510	0.0510	0.0112	0.1669	0.1668	0.0517

Table 4. Vehicle 4: Steady-state error standard deviations.

	Position (m)			Fluid velocity (mm/s)		
	x	*y*	*z*	*x*	*y*	*z*
LKF	0.0278	0.1476	0.0332	0.3193	1.5112	1.7051
EKF	0.0314	0.1674	0.0332	0.4368	2.1864	1.7050
UKF	0.0314	0.1674	0.0332	0.4368	2.1863	1.7050
BCRB	0.0167	0.0884	0.0112	0.0644	0.2833	0.0517

Table 5. Vehicle 5: Steady-state error standard deviations.

	Position (m)			Fluid velocity (mm/s)		
	x	*y*	*z*	*x*	*y*	*z*
LKF	0.1017	0.1363	0.0331	1.0335	1.2506	1.6960
EKF	0.1096	0.1468	0.0331	1.5320	1.8945	1.6953
UKF	0.1096	0.1468	0.0331	1.5320	1.8945	1.6953
BCRB	0.0281	0.0360	0.0112	0.0958	0.1019	0.0517

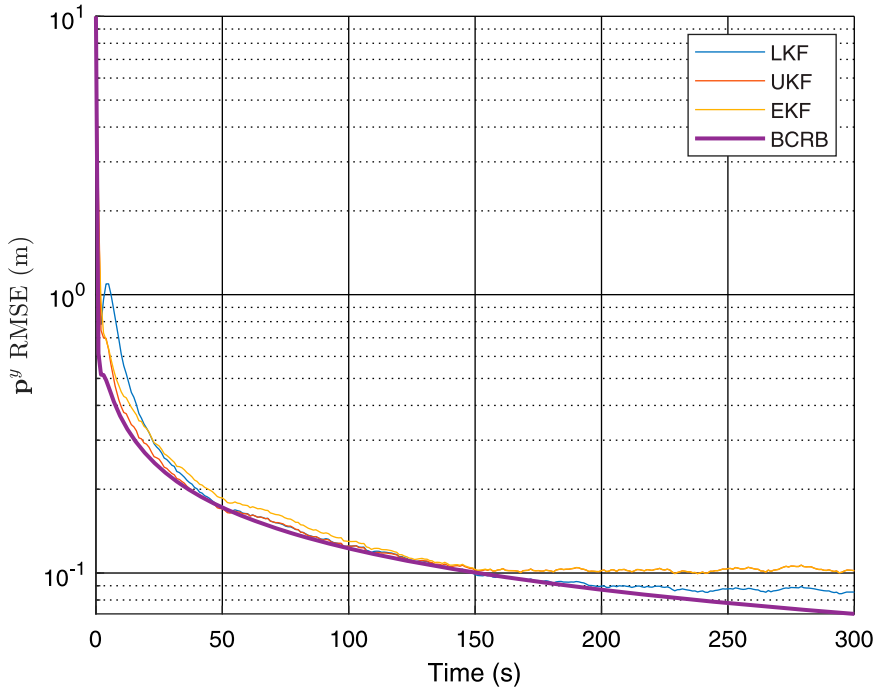

Figure 11. Vehicle 3: *y* component of position RMSE.

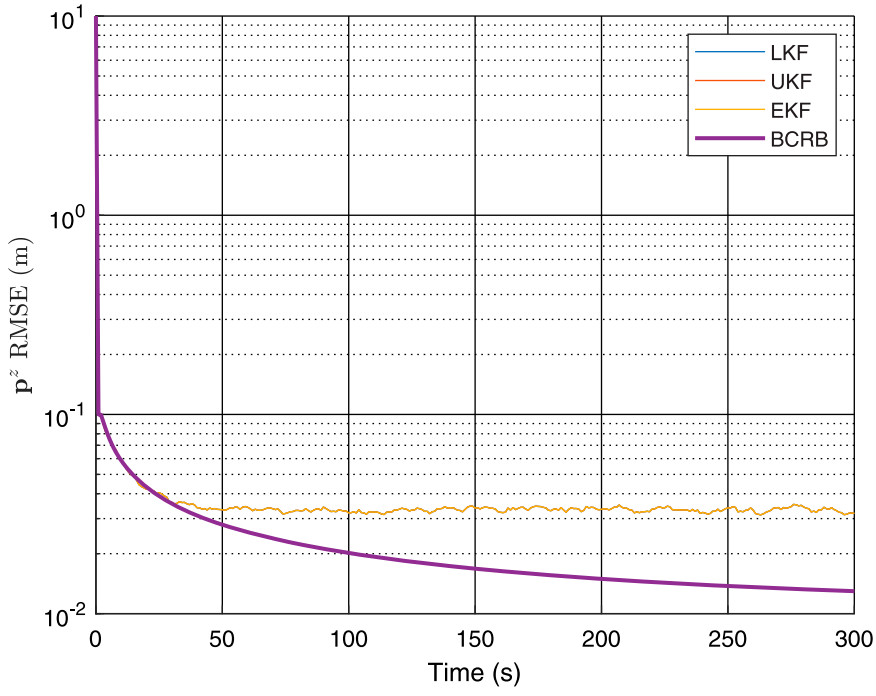

Figure 12. Vehicle 3: *z* component of position RMSE.

In conclusion, the proposed solution is slightly slower than the UKF and similar in terms of convergence speed to the EKF. At the same time, the proposed solution is clearly the one that presents lower variance in steady-state. However, these differences are not significant. As so, the proposed solution is comparable, in terms of performance, with the traditional EKF and UKF. In the next section, the advantage of the proposed solution in terms of stability, at no additional computational cost, is showcased.

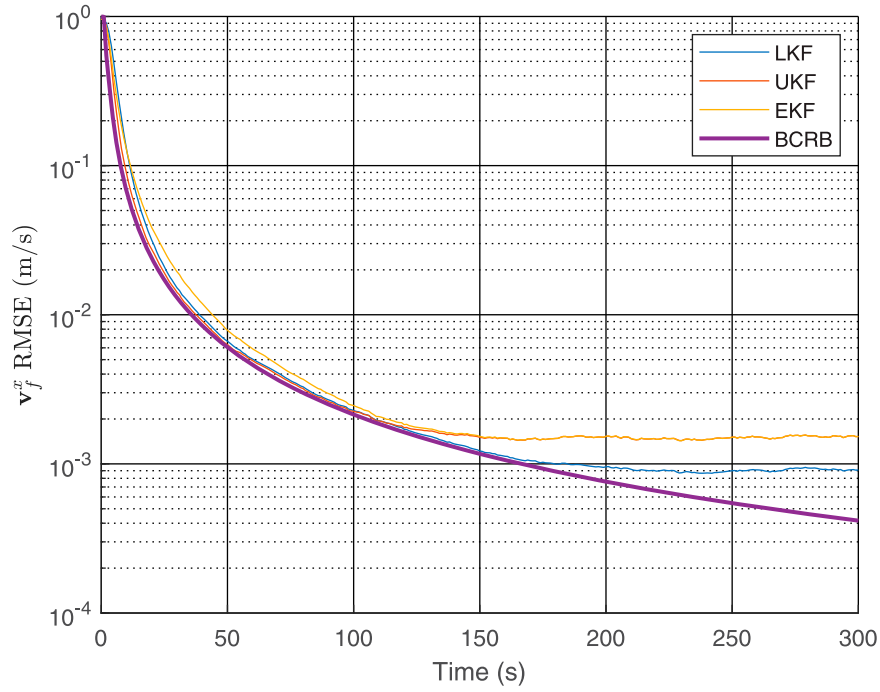

Figure 13. Vehicle 3: *x* component of fluid velocity RMSE.

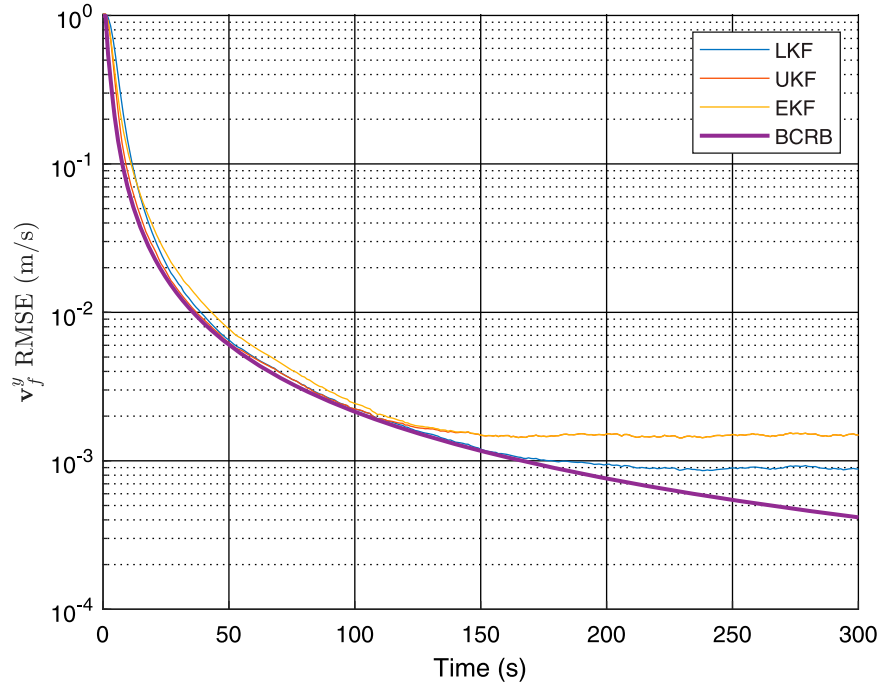

Figure 14. Vehicle 3: *y* component of fluid velocity RMSE.

Finally, it is important to remark that optimality cannot be claimed. One the one hand, and as previously mentioned, the measurement noise is not directly added to the output. On the other hand, the measurement noise appears in the output system matrix of the derived linear time-varying system. Nevertheless, the simulation results clearly show the goodness of the proposed solution, which achieves

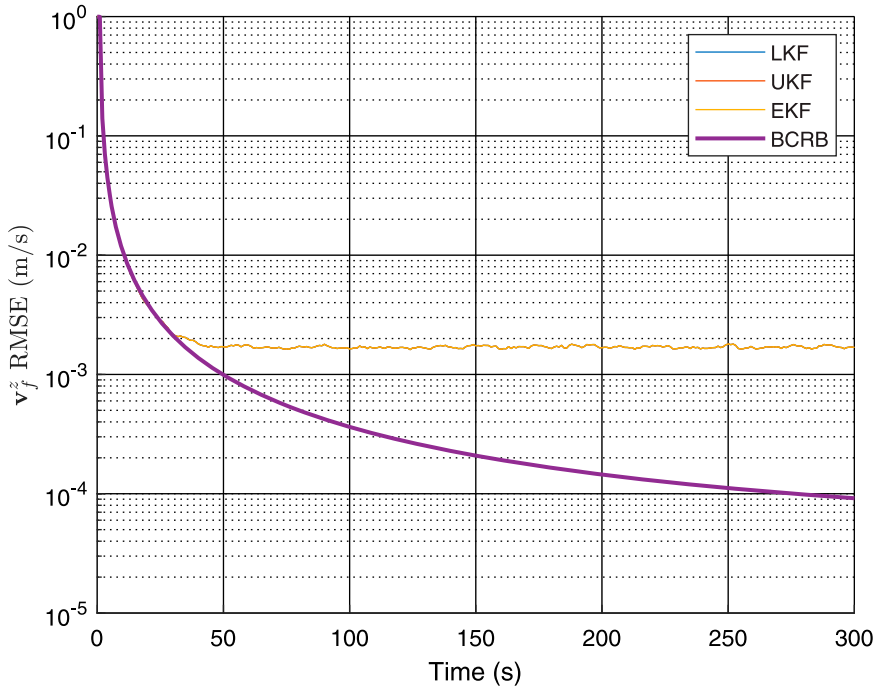

Figure 15. Vehicle 3: *z* component of fluid velocity RMSE.

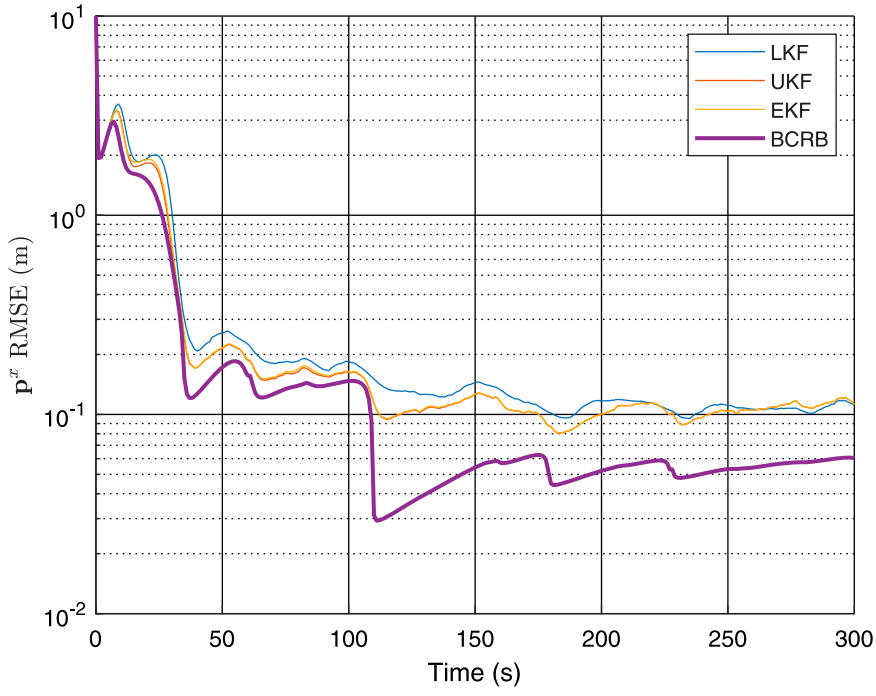

Figure 16. Vehicle 6: *x* component of position RMSE.

a RMSE close to the BCRB, which is the best possible performance achievable by any unbiased estimator.

5.4. Divergence example

The proposed solution has the advantage of exhibiting theoretical guarantees of convergence. To show

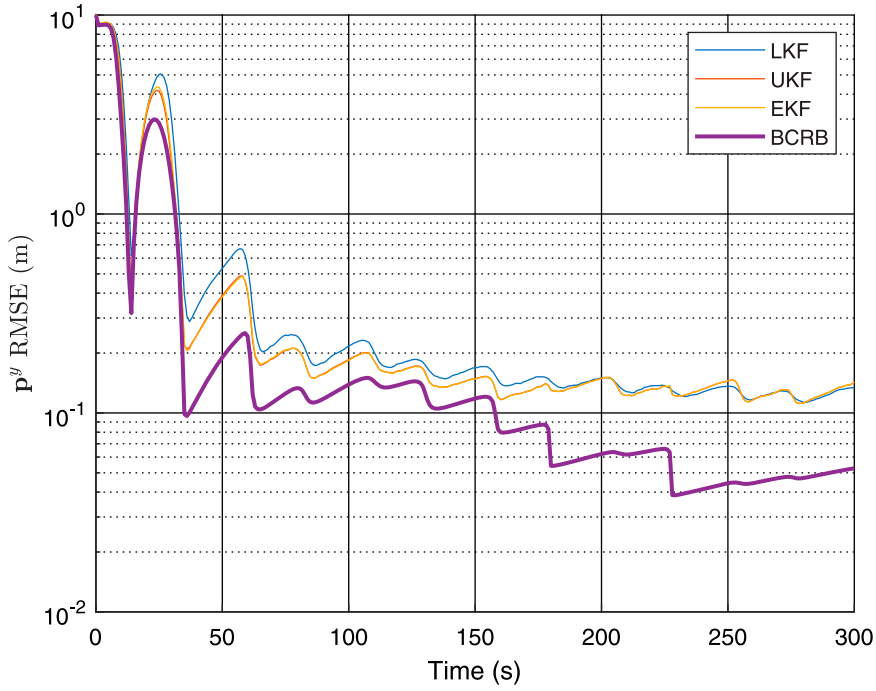

Figure 17. Vehicle 6: *y* component of position RMSE.

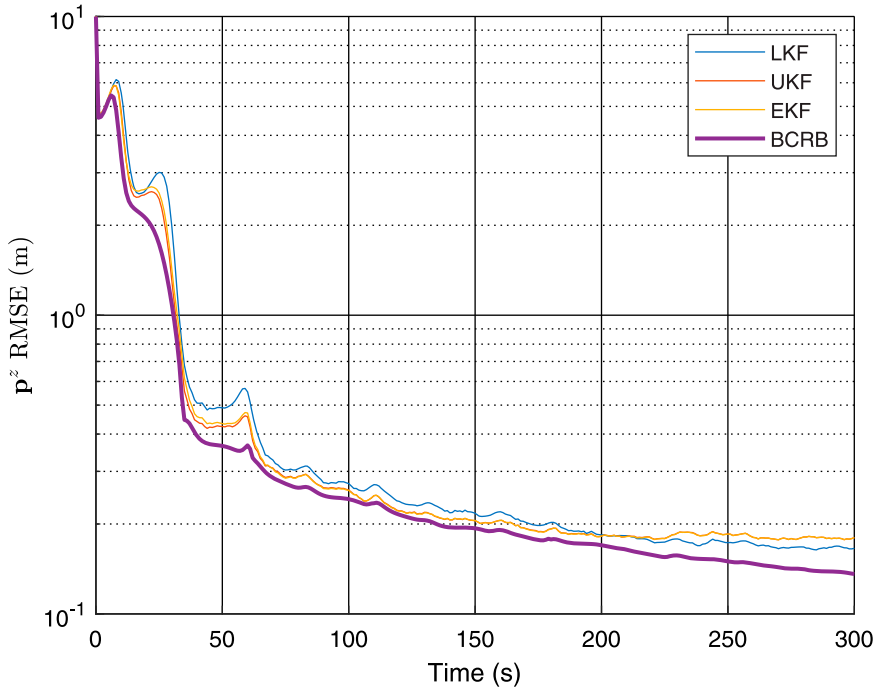

Figure 18. Vehicle 6: *z* component of position RMSE.

an example where this theoretical guarantee translates into a practical advantage, a simulation was performed in which the filters for vehicle 5 were initialised with a significant error of $[2000, 2000, 2000, 0, 0, 0]^{\mathrm{T}}$. The results for the proposed solution can be seen in Figure 22, while the results for the EKF and the UKF can be seen in Figures 23 and 24, respectively. The proposed solution is the only that converges.

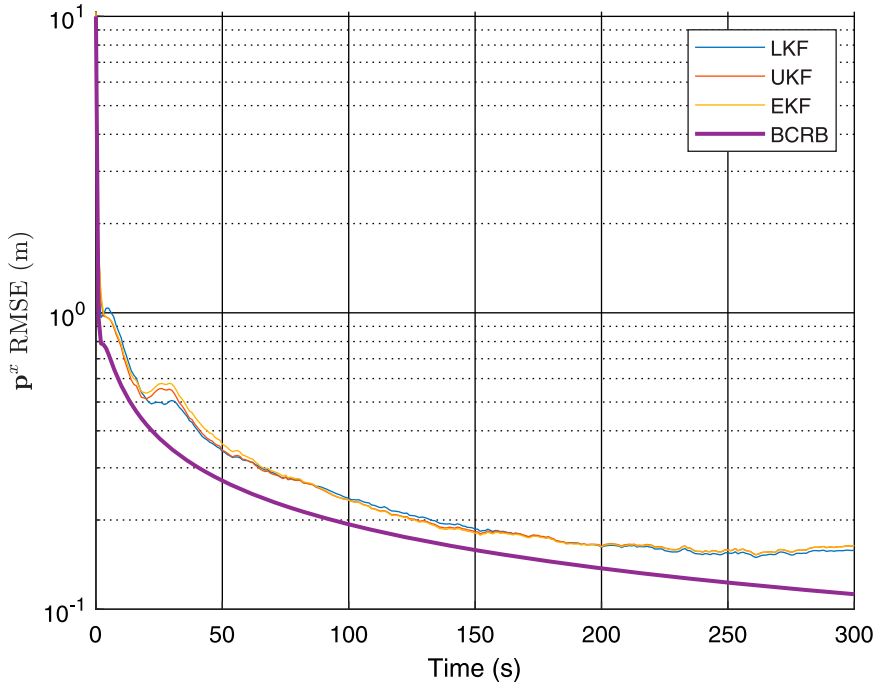

Figure 19. Vehicle 7: *x* component of position RMSE.

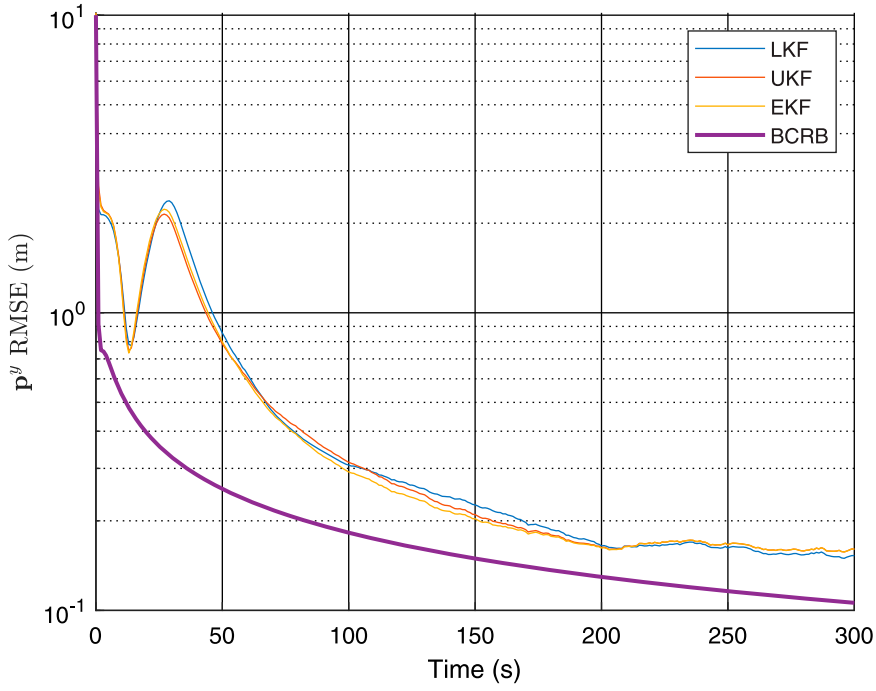

Figure 20. Vehicle 7: *y* component of position RMSE.

6. Conclusions

The communication bandwidth is very limited in underwater scenarios, rendering centralised navigation solutions impossible to implement. This paper presented a cooperative, decentralised navigation solution for formations of underwater vehicles based on bearing measurements. Three cases of interest were analysed: (i) in the first, a vehicle has access to its depth and bearing to another vehicle of the formation; (ii) in the second, the vehicle has access to bearings to at least two other vehicles of the formation; (iii) in the third, the vehicle measures the bearing relative to another vehicle but does not measure depth. In order to cope

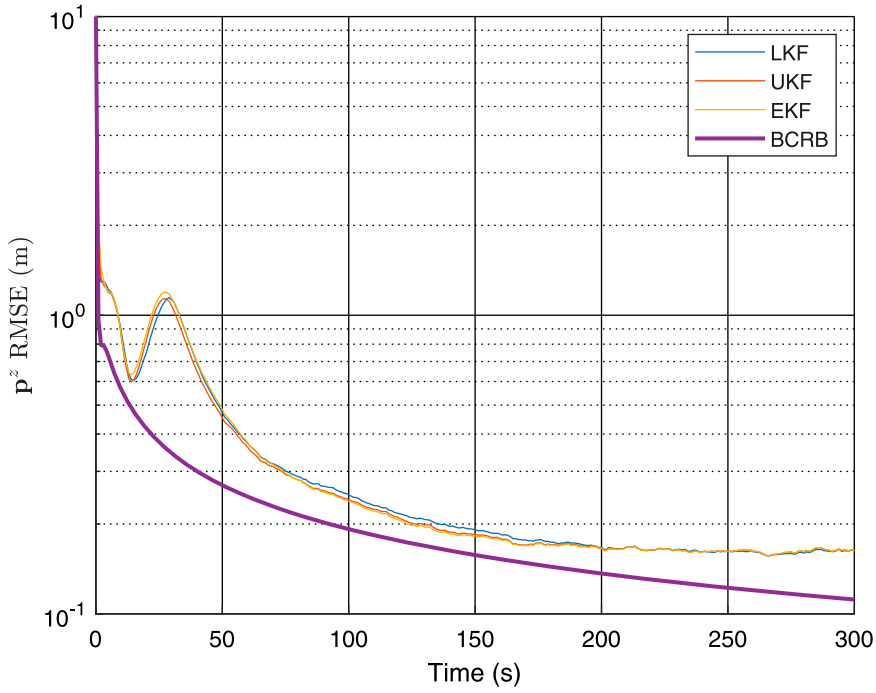

Figure 21. Vehicle 7: z component of position RMSE.

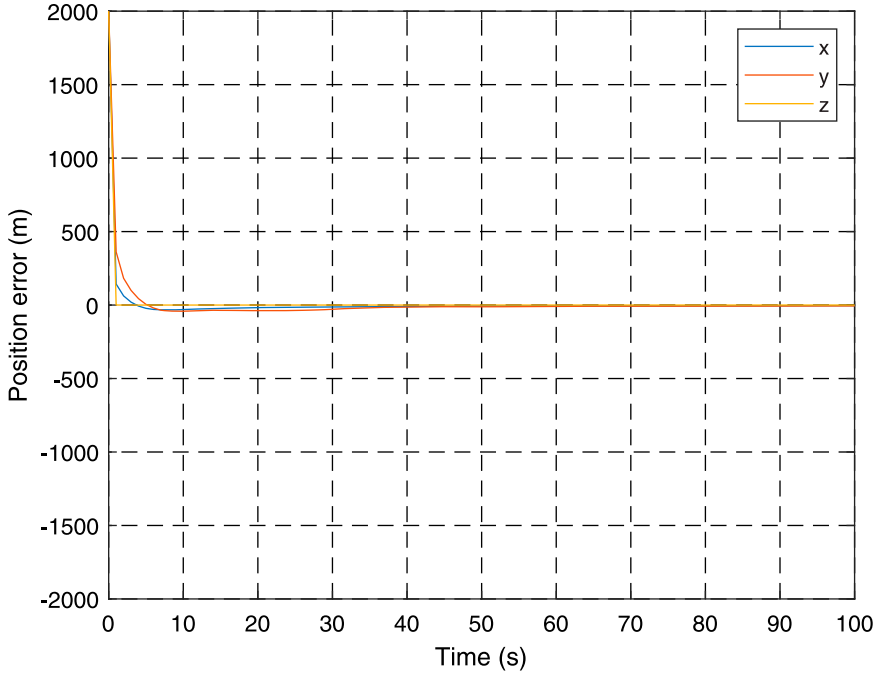

Figure 22. Vehicle 5: Convergence with LKF – Transient State.

with the nonlinear nature of the outputs, artificial outputs were employed that render the dynamics linear, thus allowing for the design of local Kalman filters with GES errors dynamics. Then, the error dynamics of the formation as a whole were also shown to be GES. The proposed design is both decentralised and distributed. On the one hand, each vehicle only estimates its own state – no vehicle estimates the whole state of the formation. On the other hand, there is no need for any centralised operation, and there is no central node. Finally, Monte Carlo simulations were presented, including the comparison with the EKF, the UKF, and the BCRB. This comparison displayed an equivalent performance level for all solutions. An

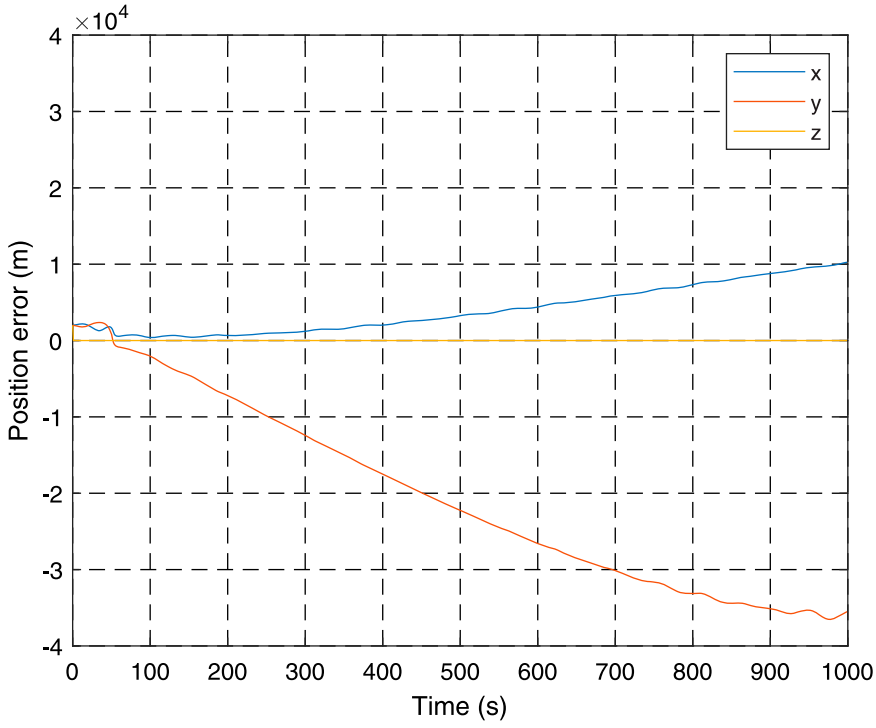

Figure 23. Vehicle 5: Convergence issues with EKF.

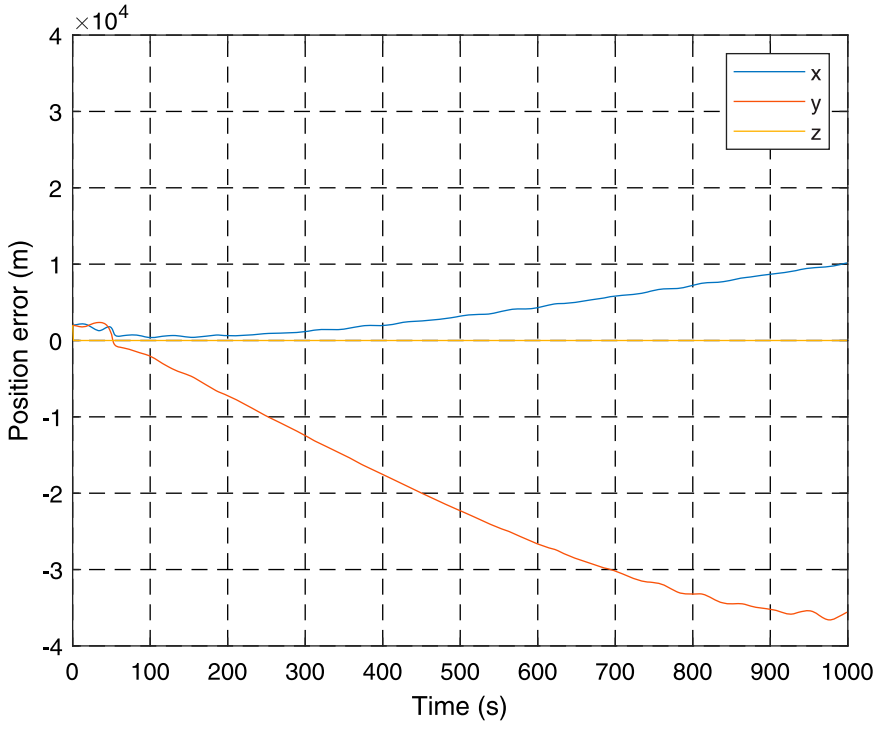

Figure 24. Vehicle 5: Convergence issues with UKF.

Table 6. Vehicle 6: Steady-state error standard deviations.

	Position (m)			Fluid velocity (mm/s)		
	x	*y*	*z*	*x*	*y*	*z*
LKF	0.1023	0.1208	0.1660	1.0192	1.0545	1.4109
EKF	0.1027	0.1302	0.1816	1.5422	1.7753	2.2076
UKF	0.1027	0.1302	0.1816	1.5421	1.7753	2.2074
BCRB	0.0289	0.0384	0.0968	0.1032	0.1355	0.3092

Table 7. Vehicle 7: Steady-state error standard deviations.

	Position (m)			Fluid velocity (mm/s)		
	x	*y*	*z*	*x*	*y*	*z*
LKF	0.1560	0.1542	0.1614	1.8748	1.8790	1.9927
EKF	0.1604	0.1605	0.1625	2.0628	2.1108	2.2128
UKF	0.1604	0.1605	0.1625	2.0636	2.1109	2.2127
BCRB	0.0802	0.0757	0.0797	0.2574	0.2433	0.2558

example that showed the advantage of the theoretical guarantee of convergence of the proposed solution was presented, making it the best solution of the three, at no additional computational cost.

Disclosure statement

No potential conflict of interest was reported by the author(s).

Funding

This work was supported by the Fundação para a Ciência e a Tecnologia (FCT) through LARSyS - FCT Project UIDB/50009/2020 and through the FCT project DECENTER [LISBOA-01-0145-FEDER-029605], funded by the Lisboa 2020 and PIDDAC programs; and by the Macau Science and Technology Development Fund under grants FDCT/0146/2019/A3 and FDCT/0031/2020/AFJ. This work has received funding from the European Union's Horizon 2020 research and innovation programme under grant agreement No. 101017808 (RAMONES project). The work of Paulo Oliveira is financed by national funds through the FCT, through IDMEC, under LAETA, project UIDB/50022/2020.

Notes on contributors

David Santos received the Mestrado Integrado degree in Aerospace Engineering, in 2020 from the Instituto Superior Técnico (IST), Lisbon, Portugal. Since 2019, he has been working in the Industry as a Data Scientist for Feedzai. His main research interests fall in the area of distributed control, computer vision and artificial intelligence.

Pedro Batista received the Licenciatura degree in Electrical and Computer Engineering, in 2005, and the PhD degree, in 2010, both from the Instituto Superior Técnico (IST), Lisbon, Portugal. From 2004 to 2006, he was a Monitor with the Department of Mathematics, IST. Since 2012, he has been with the Department of Electrical and Computer Engineering of IST, where he is currently Assistant Professor. His research interests include sensor-based navigation and control of single and multiple autonomous vehicles. Dr. Batista received the Diploma de Mérito twice during his graduation and his PhD thesis was distinguished with the Best Robotics PhD Thesis Award by the Portuguese Society of Robotics.

Paulo Oliveira (SM IEEE) received the PhD degree in Electrical and Computer Engineering, in 2002, and the Habillitation in Mechanical Engineering in 2016, all from Instituto Superior Técnico (IST), Lisbon, Portugal. Since 2020, he holds a joint position as Full Professor in the Mechanical Engineering and Eletrotechnical and Computer Engineering Departments of IST, is the Vice-president for the Research Affairs at the Associated Laboratory for Energy, Transports, and Aeronautics, and the Coordinator on Aerospace Engineering, at IST. His research interests are on Autonomous Robotic Vehicles with a focus on Mechatronic Systems Integration, Sensor Fusion, GPS and Positioning Systems, and Guidance, Navigation and Control Systems (GNC). He is author or co-author of more than 90 journal papers (90% in first quartile,) and 180 conference communications and participated in more than 40 European and Portuguese research projects, over the last 30 years.

Carlos Silvestre received the Licenciatura degree in Electrical Engineering from the Instituto Superior Técnico (IST) of Lisbon, Portugal, in 1987 and the Master degree in Electrical Engineering and the PhD degree in Control Science from the same school in 1991 and 2000, respectively. In 2011 he received the Habilitation in Electrical Engineering and Computers also from IST. Since 2000, he is with the Department of Electrical Engineering of the Instituto Superior Técnico, where he is currently on leave. Since 2012 he is also with Faculty of Science and Technology of the University of Macau where he currently holds a Professor position with the Department of Electrical and Computers Engineering. His current research interests include linear and nonlinear control theory; hybrid systems; multi-agent control systems; networked control systems; inertial navigation systems and real time architectures for complex autonomous systems with application to unmanned air and underwater vehicles.

References

Batista, P., Silvestre, C., & Oliveira, P. (2011, August). Single range aided navigation and source localization: Observability and filter design. *Systems & Control Letters*, *60*(8), 665–673. https://doi.org/10.1016/j.sysconle.2011.05.004

Batista, P., Silvestre, C., & Oliveira, P (2013a, December). GES source localization and navigation based on discrete-time bearing measurements. In *Proceedings of the 52nd IEEE Conference on Decision and Control* (pp. 5066–5071). IEEE. https://ieeexplore.ieee.org/document/6760684

Batista, P., Silvestre, C., & Oliveira, P. (2013b, November). Globally exponentially stable filters for source localization and navigation aided by direction measurements. *Systems & Control Letters*, *62*(11), 1065–1072. https://doi.org/10.1016/j.sysconle.2013.07.010

Batista, P., Silvestre, C., & Oliveira, P. (2015, October). Navigation systems based on multiple bearing measurements. *IEEE Transactions on Aerospace and Electronic Systems*, *51*(4), 2887–2899. https://doi.org/10.1109/TAES.2015.140515

Brehard, T., & Cadre, J. L. (2007, October). Hierarchical particle filter for bearings-only tracking. *IEEE Transactions on Aerospace and Electronic Systems*, *43*(4), 1567–1585. https://doi.org/10.1109/TAES.2007.4441759

Fonti, A., Freddi, A., Longhi, S., & Monteri, A (2011, August–September). Cooperative and decentralized navigation of autonomous underwater gliders using predictive control. In *Proceedings of the 18th IFAC World Congress* (pp. 12813–12818). https://www.sciencedirect.com/science/article/pii/S1474667016456788

Hammel, S., & Aidala, V. (1985, March). Observability requirements for three-dimensional tracking via angle measurements. *IEEE Transactions on Aerospace and Electronic Systems*, *21*(2), 200–207. https://doi.org/10.1109/TAES.1985.310617

Healey, A. J. (2001, December). Application of formation control for multi-vehicle robotic minesweeping. In *Proceedings of the 40th IEEE Conference on Decision and Control* (pp. 1497–1502). IEEE. https://ieeexplore.ieee.org/document/981106

Hu, G., Gao, S., & Zhong, Y. (2015, May). A derivative UKF for tightly coupled INS/GPS integrated navigation. *ISA Transactions*, *56*(4), 135–144. https://doi.org/10.1016/j.isatra.2014.10.006

Jazwinski, A. (1970). *Stochastic processes and filtering theory*. Academic Press.

Joordens, M. A., & Jamshidi, M. (2010, May). Consensus control for a system of underwater swarm robots. *IEEE Systems Journal*, *4*(1), 65–73. https://doi.org/10.1109/JSYST.2010.2040225

Kopfstedt, T., Mukai, M., Fujita, M., & Ament, C (2008, July). Control of formations of UAVs for surveillance and reconnaissance missions. In *Proceedings of the 17th IFAC World Congress* (pp. 5161–5166). https://www.sciencedirect.com/science/article/pii/S1474667016397622

Pack, D. J., DeLima, P., Toussaint, G. J., & York, G. (2009, August). Cooperative control of UAVs for localization of intermittently emitting mobile targets. *IEEE Transactions on Systems, Man, and Cybernetics–Part B: Cybernetics*, *39*(4), 959–970. https://doi.org/10.1109/TSMCB.2008.2010865

Reis, J., Morgado, M., Batista, P., Oliveira, P., & Silvestre, C. (2016, September). Design and experimental validation of a USBL underwater acoustic positioning system. *Sensors*, *16*(9), 1491. https://doi.org/10.3390/s16091491

Santos, D., & Batista, P (2020, July). Decentralized navigation systems for bearing-based position and velocity estimation in tiered formations. In *Proceedings of the 2020 American Control Conference* (pp. 5225–5230). https://ieeexplore.ieee.org/document/9147640

Stilwell, D. J., & B. E. Bishop (2000, December). Platoons of underwater vehicles. *IEEE Control Systems Magazine*, *20*(6), 45–52. https://doi.org/10.1109/37.887448

Techy, L., Morgansen, K., & Woolsey, C (2011, June–July). Long-baseline acoustic localization of the Seaglider underwater glider. In *Proceedings of the 2011 American Control Conference* (pp. 3990–3995). https://ieeexplore.ieee.org/document/5991416

Vaccarani, M., & Longhi, S (2009, June). Formation control of marine vehicles via real-time Networked Decentralized MPC. In *Proceedings of the 17th Mediterranean Conference on Control and Automation* (pp. 428–433). https://ieeexplore.ieee.org/document/5164579

van Trees, H. (2007). *Bayesian bounds for parameter estimation and nonlinear filtering/tracking*. Wiley-IEEE Press.

Viegas, D., Batista, P., Oliveira, P., & Silvestre, C. (2016, March). Decentralized state observers for range-based position and velocity estimation in acyclic formations with fixed topologies. *International Journal of Robust and Nonlinear Control*, *26*(5), 963–994. https://doi.org/10.1002/rnc.v26.5

Wan, E., & Merwe, R (2000, October). The unscented Kalman filter for nonlinear estimation. In *Proceedings of the IEEE 2000 Adaptive Systems for Signal Processing, Communications, and Control Symposium* (pp. 153–158). https://ieeexplore.ieee.org/document/882463

Whitcomb, L., Yoerger, D., & Singh, H (1999, August). Combined Doppler/LBL based navigation of underwater vehicles introduction. In *Proceedings of the 11th International Symposium on Unmanned Untethered Submersible Technology* (pp. 1–7).

Zhang, J., & Ji, J. (2012). Distributed multi-sensor particle filter for bearings-only tracking. *International Journal of Electronics*, *99*(2), 239–254. https://doi.org/10.1080/00207217.2011.623276

Zhao, X., Wang, L., He, Z., Yao, Z., & Li, R. (2014, June). Applications of square root cubature Kalman filtering to bearing only tracking. *Piezoelectrics and Acoustooptics*, *36*(3), 445–449.